2008 IEEE International Conference on
Robotics and Automation
Pasadena, CA, USA, May 19-23, 2008

Quasi-Static Rolling Control of the Rolling Disk Biped Robot

Cristian C Phipps, *Student Member, IEEE*, and Mark A. Minor, *Member, IEEE*

Abstract—**Motivated by the need for greater speed, adaptability and efficiency in legged robots, a class of hybrid robots have been developed which hybridize rolling locomotion with legged locomotion. Herein we present a quasi-static rolling control law for the hybrid climbing/rolling robot the Rolling Disk Biped. We provide experimental results comparing speed and energy consumption data for quasi-static rolling versus walking. We show that rolling can significantly improve energy efficiency over walking—by as much as a factor of 3.9.**

I. INTRODUCTION

Motivated by the need for greater speed, efficiency and adaptability in climbing and walking robots, we have developed a class of robots which hybridize climbing and walking with rolling locomotion [1-3]. The innovative morphologies of these robots allow for rolling locomotion without the need for additional resources beyond those required for climbing and walking. By increasing the available modes of locomotion, the adaptability of a mobile robot is increased because it may select the locomotion method best suited for a particular operational environment. Legged locomotion is excellent for moving through rough and unstructured terrain, but is slow and demanding of energy. Rolling is apt to higher speeds and is more energy efficient (especially on downhill slopes) but requires smoother, better structured environments.

Herein we prove that rolling modes of locomotion on such hybrid robots are capable of greater energy efficiencies than walking modes. The quasi-static rolling locomotion control we have developed and tested in this paper is capable of improving energy efficiency by as much as a factor of 3.9 over walking on the Rolling Disk Biped (RDB) robot when magnets are used as grippers. The motors alone may use 14% less energy for rolling than the most efficient walking gait evaluated here.

The RDB is a three degree-of-freedom planar robot which serves as a two dimensional test-bed for our studies in the hybridization of climbing and rolling and the control thereof. Refer to [1, 2] for details of its design. Experience with the RDB will be applied towards future design iterations of the RDB and the spherical hexapod robot Hex-A-Ball (HAB) [3], both which are anticipated to extend the capabilities of the current RDB into E^3.

Our quasi-static rolling controller (introduced in [3]) works by slowly moving the robot's center of gravity (CG) about its geometric center through coordinated joint movements; if the CG is moved sufficiently slowly, the robot should roll to maintain equilibrium. Other robots have demonstrated the success of similar CG offset rolling methods such as those by Halme [4], Mukherjee [5], Yim [6], Yamawaki [7], and Lee [8].

A controller such as the one we present here is best suited for passive stabilization at a desired orientation and for slower rolling locomotion (0-0.083 rev/s on the RDB) and positioning where inertial effects are mostly negligible. Feed-forward joint paths are calculated offline using a static optimization routine to find joint angles whose effect is to cause the net robot CG path to track a reference orbit about the geometric center of the robot at a specified radius. Such joint paths are generated for radii between 2 and 8 mm and are played back at rates between 10°/s and 30°/s. We compare experimental results of these rolling trajectories and evaluate energy efficiency and trajectory tracking characteristics. We also compare these rolling locomotion results against rudimentary walking locomotion data obtained for the RDB prototype.

The controller presented here is an improvement over the model based controller of [1, 2] which was not capable of reproducing expected results. The controller in [1, 2] uses polynomial joint trajectories to create a net change in the RDB's CG position; simulations are used to manually tune the polynomial parameters such that an entire revolution of the RDB results. A likely cause for the failure of this controller to produce expected results is discrepancies between model parameters used in the simulations and those of the actual system—especially viscous friction parameters.

It will be shown that the quasi-static rolling locomotion controller we have developed is capable of producing nearly an entire revolution of the RDB robot and tracking a rolling angle reference reasonably well. Further, we will show that this rolling method is capable of increasing energy efficiency on a distance basis by as much as a factor of 3.9.

We begin this paper with a description of the kinematic model of the RDB in Section II. Our quasi-static rolling locomotion controller is detailed in Section III. We present and discuss our experimental results in Section IV. Conclusions and discussion of future work is contained in Section V.

Manuscript received September 13, 2007.

C. C Phipps is with the University of Utah Department of Mechanical Engineering, Salt Lake City, UT 84101 USA (phone: 801-587-9018; fax: 801-585-9826; e-mail: cristianphipps@gmail.com).

M. A. Minor is with the University of Utah Department of Mechanical Engineering, Salt Lake City, UT 84101 USA (e-mail: minor@mech.utah.edu).

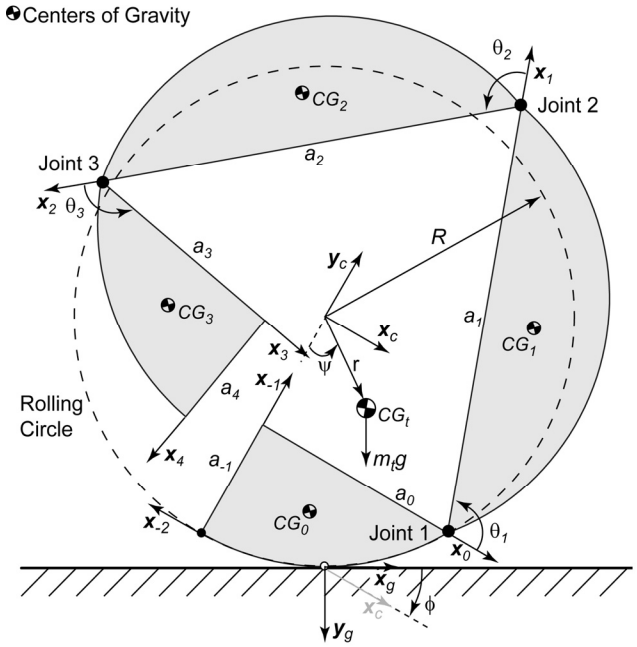

Fig. 1. Kinematic model of the RDB used for rolling locomotion analyses.

TABLE 1
VALUES FOR DH AND INERTIAL PARAMETERS USED IN CALCULATIONS AND APPEARING IN FIG. 1

i	a_i (mm)	θ_i (deg)	m_i (g)	${}^i\mathbf{b}_i$ (mm)
-1	48	-90	Na	Na
0	84	*	182	$[-51\ -23\ 1]^T$
1	167	*	363	$[-84\ -21\ 1]^T$
2	167	*	376	$[-90\ -18\ 1]^T$
3	84	*	209	$[-36\ -21\ 1]^T$
4	48	-90	Na	Na

II. ROLLING DISK BIPED KINEMATICS

The net CG location of the RDB is determined from the relative positions of its links. The standard Denavit-Hartenberg (DH) convention [9] is used for kinematic parameterization of the RDB. Fig. 1 identifies the DH parameters on a kinematic drawing of the RDB. Frame *c* locates the center of the Rolling Circle which is coincident with the center of the circular rolling surface of the grounded link and is fixed with respect to that link. Frame *g* locates the ground contact point where $\mathbf{y}_g$ is defined as the normal to the rolling surface and $\mathbf{z}_g$ points into the plane. The Rolling Angle ϕ is the rotation of frame *c* about $\mathbf{z}_g$.

The CG location ${}^c\mathbf{r}$ expressed in frame *c* is found in homogeneous coordinates using:

$$
{}^c\mathbf{r} = \begin{cases}
\dfrac{{}^c\mathbf{T}_0}{m_t}\left[m_0\,{}^0\mathbf{b}_0 + m_1\,{}^0\mathbf{T}_1\,{}^1\mathbf{b}_1 + m_2\,{}^0\mathbf{T}_2\,{}^2\mathbf{b}_2 + m_3\,{}^0\mathbf{T}_3\,{}^3\mathbf{b}_3\right] \\
\qquad \text{for } 0^\circ \le \phi < 60^\circ \\
\dfrac{{}^c\mathbf{T}_1}{m_t}\left[m_0\,{}^1\mathbf{T}_0\,{}^0\mathbf{b}_0 + m_1\,{}^1\mathbf{b}_1 + m_2\,{}^1\mathbf{T}_2\,{}^2\mathbf{b}_2 + m_3\,{}^1\mathbf{T}_3\,{}^3\mathbf{b}_3\right] \\
\qquad \text{for } 60^\circ \le \phi < 180^\circ \\
\dfrac{{}^c\mathbf{T}_2}{m_t}\left[m_0\,{}^2\mathbf{T}_0\,{}^0\mathbf{b}_0 + m_1\,{}^2\mathbf{T}_1\,{}^1\mathbf{b}_1 + m_2\,{}^2\mathbf{b}_2 + m_3\,{}^2\mathbf{T}_3\,{}^3\mathbf{b}_3\right] \\
\qquad \text{for } 180^\circ \le \phi < 300^\circ \\
\dfrac{{}^c\mathbf{T}_3}{m_t}\left[m_0\,{}^3\mathbf{T}_0\,{}^0\mathbf{b}_0 + m_1\,{}^3\mathbf{T}_1\,{}^1\mathbf{b}_1 + m_2\,{}^3\mathbf{T}_2\,{}^2\mathbf{b}_2 + m_3\,{}^3\mathbf{b}_3\right] \\
\qquad \text{for } 300^\circ \le \phi < 360^\circ
\end{cases} \tag{1}
$$

where ${}^i\mathbf{T}_j$ is a homogeneous transformation matrix representing the coordinate transformation from frame *j* to *i*, and ${}^i\mathbf{b}_i$ is the homogeneous coordinate of the CG of link *i* in frame *i*. The mass of link *i* is m_i, and the total mass is $m_t = m_0 + m_1 + m_2 + m_3$. Table 1 provides numerical values for the constants appearing in the above equations and in Fig. 1.

Important quantities used extensively through the rest of this paper are the CG Offset Length L

$$L = \sqrt{{}^c r_1^2 + {}^c r_2^2} \tag{2}$$

and the CG Offset Angle ψ

$$\psi = \operatorname{atan2}({}^c r_2, {}^c r_1) + 90^\circ \tag{3}$$

where the coefficients ${}^c r_1$ and ${}^c r_2$ are the first and second elements of ${}^c\mathbf{r}$ respectively.

III. QUASI-STATIC ROLLING CONTROL

Assuming rolling resistances and inertial effects to be negligible, gravity will cause the RDB to settle to the orientation in which its CG is directly above its ground contact point, resulting in static equilibrium. If the CG position is slowly perturbed, the RDB will roll to restore equilibrium. This principle is illustrated in Fig. 2. Our assumptions allow us to further assume that the orientation the RDB settles to is independent of the CG Offset Length L ($L \neq 0$), and only dependent on the CG Offset Angle ψ. Hence, $\psi = 0 \rightarrow 360^\circ$ will produce a full rotation of the

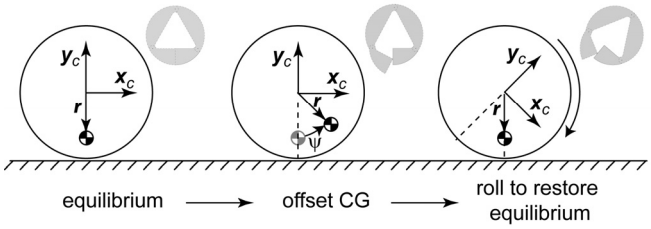

Fig. 2. Quasi-static rolling principle. The shaded figures in the upper-right of each frame show sample RDB configurations for each instance.

RDB if $L > 0$ for all ψ. Realistically however, the larger *L* is, the greater the control authority and stability of the orientation.

A. Generation of Joint Paths by CG Offset Length Optimization

Our quasi-static rolling control strategy is to generate joint paths which produce CG Offset Length paths ($L > 0$) for CG Offset Angles $\psi = 0^\circ \rightarrow 360^\circ$. The joint paths are then used as feed-forward control inputs to the joint servos, played back at various rates. We treat the generation of these paths as a sequence of constrained optimization problems where our objective is to find joint angles, $\boldsymbol{\theta}_k$, which maximize CG Offset Length, L_k, at discreet points, ϕ_k, of the Rolling Angle path. The subscript *k* is introduced to denote the k^{th} optimization problem. Matlab's™ *fmincon* function is used to sequentially solve each *k* optimization problem where the joint positions resulting from optimization *k* are used as initial estimates for optimization *k*+1. The optimization constraints are detailed below.

Maximum CG Offset Length: The CG Offset Length L_k, calculated using (2), is constrained to some Maximum CG Offset Length L_{max}. This is accomplished with the inequality constraint

$$0 \geq L_k - L_{max} \tag{4}$$

CG Offset Angle: For any desired Rolling Angle ϕ_k, the CG Offset Angle ψ_k, calculated using (3), must match, resulting in the equality constraint

$$0 = \phi_k - \psi_k \tag{5}$$

Rolling Surface Continuity: Ensuring continuity in the RDB's rolling surface requires that the joint variables be constrained to their nominal positions when the Rolling Angle is near the angles corresponding to the joint locations and the terminal ends of the robot, i.e. $\phi_{crit} = \{0^\circ, 60^\circ, 180^\circ, 300^\circ, 360^\circ\}$. The hyperbolic-tangent function is used to constrain the joint variables within an envelope according to

$$0 = \theta_i - \left(\theta_{nom} + \Delta\theta_{k,i} \left| \tanh\left(-180^0 \frac{\phi_k - \phi_{crit,n}}{\phi_{smooth,n} - \phi_{crit,n}} \right) \right| \right) \tag{6}$$

where $\theta_{nom} = 120^\circ$ is the nominal joint angle for all joints (perfect circle configuration), $\Delta\theta_{k,i}$ is the deviation from the nominal value for joint *i* constrained to $-\Delta\theta_{allow} \leq \Delta\theta_{k,i} \leq \Delta\theta_{allow}$, where $\Delta\theta_{allow}$ is determined by the physical angular limit of the joints. ϕ_k is the desired Rolling Angle and $-\phi_{smooth} = \phi_{crit} - 30^\circ$ is the Rolling Angle at which the envelope begins to narrow as ϕ_{crit} is approached; 30° was chosen because it is the largest value that allows the envelope to open to its maximum value between ϕ_{crit} = 0° and 60° (similarly between ϕ_{crit} = 300° and 360°). The value of index *n* is determined by the desired Rolling Angle as

$$n = \begin{cases} 1 & \text{for} \quad 0^\circ \leq \phi_k < 30^\circ \\ 2 & \text{for} \quad 30^\circ \leq \phi_k < 120^\circ \\ 3 & \text{for} \quad 120^\circ \leq \phi_k < 240^\circ \\ 4 & \text{for} \quad 240^\circ \leq \phi_k < 330^\circ \\ 5 & \text{for} \quad 330^\circ \leq \phi_k \leq 360^\circ \end{cases} \tag{7}$$

Foot-Against-Foot Interference: For any desired Rolling Angle, the RDB is limited to joint configurations which do not result in collisions between the feet. The magnitude of a foot collision is quantified by comparing the distances from the edges of Foot One (O_{-2} and O_{-1}) to Foot Two (O_3 and O_4). A collision is determined to have occurred if

$$\begin{gathered} 0 \leq {}^0\mathbf{x}_0 \cdot {}^0\mathbf{d}_{ij} \\ \text{and} \\ 0 \leq {}^0\mathbf{x}_3 \cdot {}^0\mathbf{d}_{ij} \end{gathered} \tag{8}$$

where ${}^0\mathbf{d}_{ij}$ is the inter-origin vector from frame *i* to *j* expressed in frame 0 for *i*={-1,-2} and *j*={3,4}. This principle is illustrated in Fig. 3. Relevant parameters are listed in Table 1 and may be used to determine the locations of the coordinate frame origins representing the foot edges.

A numerical value describing the relative closeness of the foot surfaces to one another may be found by

$$u_{ij} = \begin{cases} {}^0\mathbf{x}_0 \cdot {}^0\mathbf{d}_{ij} & \text{if} \quad 0 \leq {}^0\mathbf{x}_3 \cdot {}^0\mathbf{d}_{ij} \\ {}^0\mathbf{x}_3 \cdot {}^0\mathbf{d}_{ij} & \text{if} \quad 0 \leq {}^0\mathbf{x}_0 \cdot {}^0\mathbf{d}_{ij} \\ {}^0\mathbf{x}_0 \cdot {}^0\mathbf{d}_{ij} + {}^0\mathbf{x}_3 \cdot {}^0\mathbf{d}_{ij} & \text{else} \end{cases} \tag{9}$$

where negative values for u_{ij} indicate no collision and positive values indicate a collision. The resulting inequality constraints are

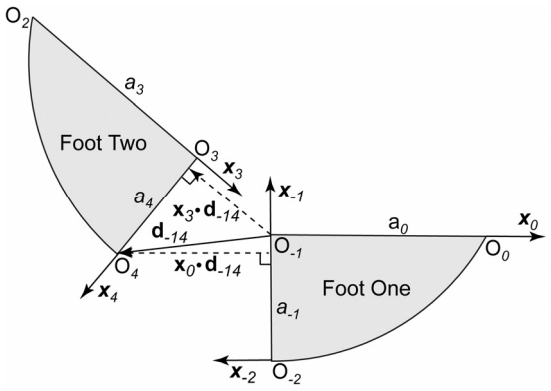

Fig. 3. Illustration of foot collision quantification concept.

$$0 \geq u_{ij} \text{ for } i = \{-1,-2\},\ j = \{3,4\}\ . \tag{10}$$

Sample joint path generation results are portrayed in Fig. 4 which shows joint and CG paths for allowed Max. CG Offset Lengths of 2 and 8 mm. It can clearly be seen that our joint path generation routine was successful in producing continuous joint paths which result in CG Offset Length paths of nearly constant value at the desired Max. CG Offset Lengths. The exception is at CG Offset Angles near ϕ_{crit} where the rolling surface continuity constraint causes the CG Offset Length to dip towards zero. Though we neglect inertial effects in the development of our quasi-static control law, we assume that enough momentum and gravitational effects due to system lag will be present in experimentation to carry the robot past ϕ_{crit} .

The rolling surface continuity constraint also causes Joints 1 and 3 to displace rapidly near ϕ_{crit} which might introduce unwanted dynamic effects. However, by inspection, their accelerations are nearly equal and in opposite directions which helps to cancel out their net dynamic effect. These rapid joint displacements also place limits on how fast the joint paths may be played back on the robot which has a limited joint angle rate—large gear ratios are required for climbing and restrict the amount of motor power available as speed.

Notice also that the joint paths for different Max. CG Offset Lengths have very similar shapes and are nearly scaled versions of each other, larger Max. CG Offset Lengths requiring larger joint deviations. A major implication of this is that more energy will be required to run larger Max. CG Offset paths, as they require greater joint articulations.

IV. Results

A. Experimental Setup

Walking and rolling experiments are performed using the RDB robot and a dSpace 1103 controller board is used for

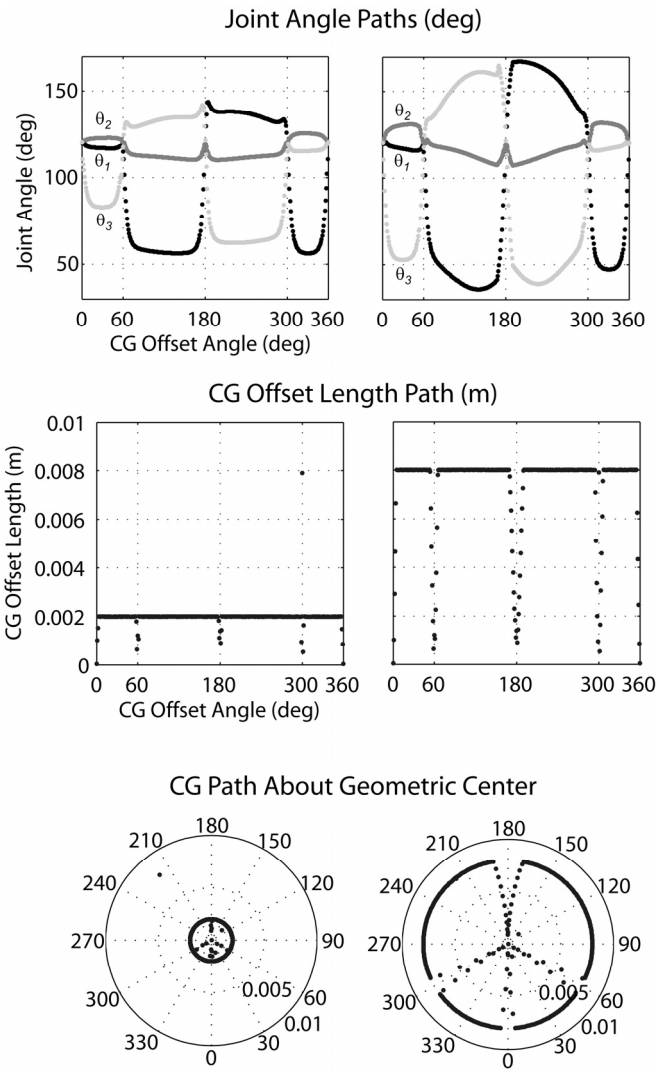

Fig. 4. Results of joint path generation for Maximum CG Offset Lengths of 2 and 8 mm. Joint paths and CG Offset Length are shown as functions of the desired CG Offset Angle. The corresponding path of the net CG about the geometric center of the rolling circle is included for each set of joint paths.

control. PWM motor control signals from the dSpace are amplified by H-bridges, and binary gripper control signals from the dSpace control digital switches to allow current to the elctro-magnetic grippers. Power to the H-bridges and magnets is provided by a 24V 10A DC power supply. Power to the RDB's motors, magnets and potentiometers is provided via a tether, which also transmits joint position potentiometer signals to the dSpace.

To monitor motor and magnet power draw, current shunt resistors are connected in series on the low sides of the H-bridge power supply and magnets. Difference amplifiers are used to amplify the voltage drop across the resistors which is measured and recorded by the dSpace. For purposes of comparison between the different modes of locomotion, we choose to express energy consumption on a per meter basis. For rolling experiments, we assume exactly one revolution is completed for all experiments performed.

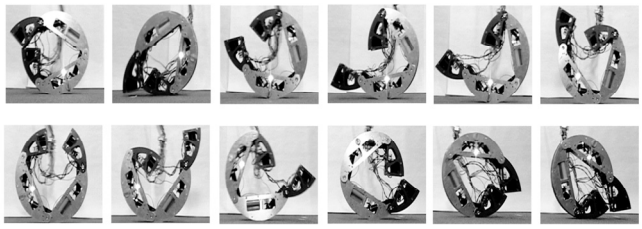

Fig. 5. Still frames of the RDB rolling one revolution (using the 8 mm Max. CG Offset Length - 30°/s CG Offset Angle Rate trajectory).

The controller for the RDB is created using Simulink 6.1 and is downloaded to the dSpace board using Matlab 7.0.1 Real-Time Workshop. The controller consists of a feed-forward joint trajectory input to a proportional control servo loop which controls the position of the three joints on the RDB. Control for the grippers is provided by feed-forward binary trajectories. A sampling rate of 1k Hz is used in the implementation of the controller.

User interface with and data collection from the dSpace 1103 board are provided by dSpace Control Desk Developer Version 2.5.6 software. Data for joint errors and motor and magnet power draw are sampled and recorded at a rate of 100 Hz. Still frame analysis of video captures is used to manually measure Rolling Angles at a rate of 12 equally spaced frames per desired revolution of the RDB, and at the final resting Rolling Angle. Analysis of our Rolling Angle measurement technique proved it to be sufficiently precise with a standard deviation in repeated measurements of 1.2° or less.

Rolling experiments are performed in our lab on unpadded industrial loop-pile carpet surfaces. Walking experiments are performed in our lab on 3/16" steel plate.

B. Level Surface Quasi-Static Rolling Experiments Using Constant CG Offset Angle Rate Trajectories

Level surface quasi-static rolling experiments are evaluated using Constant CG Angle Offset Rate (CCGOAR) trajectories. As their name implies, these trajectories produce a CG trajectory about the geometric center of the rolling circle at some constant CG Offset Angle rate. They were generated using paths of Maximum CG Offset Lengths (MCGOL) of 2, 4, 6, and 8 mm (generated as detailed in Section III.A), played at Constant CG Offset Angle Rates (CCGOAR) of 10, 20, and 30 °/s. Trajectories of MCGOL greater than 8 mm cause the robot joints to exceed their limits and are therefore not evaluated. Trajectories with CCGOAR greater than 30°/s require joint trajectories which the current RDB actuators cannot sufficiently track and are therefore not evaluated either.

Five experiments were performed for each trajectory in order to evaluate success rate (number of experiments producing maximum Rolling Angles greater than 330°). Motor power consumption and joint error data collected using the Control Desk software was analyzed for all of each set of five experiments, and still frame analysis was used on one of each set of five experiments. Refer to Fig. 5 for an example of the RDB rolling using our quasi-static control law.

The plots in Fig. 6a-d show the results of the still frame analysis providing measured Rolling Angle trajectories for MCGOL of 2, 4, 6, and 8 mm respectively. It is clearly seen that as MCGOL increases, trajectory tracking is improved as a result of the greater control authority provided by larger moments. In Table 2 we show the Rolling Angle Error RMS data, which support this observation. Also, note the perfect success rates in Table 3 for the 8 mm MCGOL trajectories, and the generally poor success rates for the 2 mm MCGOL trajectories which further support this observation.

It is also interesting to note in Fig. 6 that many of the trajectories display non-quasi-static characteristics; e.g. the 2 mm MCGOL - 30°/s CCGOAR trajectory shows periods of rapid rolling rates from still frame 2 to 4 and again from still frame 7 to 9. Such dynamic effects are in fact quite important to the success of our control law. Notice in Table 3 that perfect success rates are observed only for the 30°/s CCGOAR trajectories. Because these are the fastest of the CCGOAR trajectories, they are presumably more dynamic and it is likely because of these dynamics that these trajectories are successful while slower CCGOAR trajectories are not. This demonstrates the influence of dynamics on our quasi-static control law and implicates work in dynamic rolling control of the RDB and other such robots.

Energy consumption results are presented in Table 4 as averages of the five experiments. In general, it is seen that energy usage increases with increasing MCGOL and decreasing CCGOAR. Because of the worm gearing and large gear ratio, a large amount of the motors' effort is assumed to go into overcoming friction in the gear train. Therefore the longer the motors are run, and the larger the joint articulations (as required by larger MCGOL trajectories) the more energy will be required, as can be seen in Table 4.

Experimental results worth noting are the 10 and 20 °/s - 8 mm MCGOL trajectories which have the best Rolling Angle trajectory tracking. Because these trajectories have the largest MCGOL and the slowest CCGOAR of all trajectories examined, this result is in concert with our expectations. The larger MCGOL afford greater control authority and the slower CCGOAR make our quasi-static assumption more viable.

Another interesting result is the poor Rolling Angle tracking and success rates observed for the 2 mm MCGOL - 10 and 20 °/s CCGOAR joint trajectories. Inspection of Table 3 shows that in fact these joint trajectories are not at all reliable for rolling. Our quasi-static assumption would require that these slower trajectories work if the same joint paths played at a *faster* rate do. This observation is an indication of the beneficial role dynamic effects have on our quasi-static control law. The inability of our controller to work for these trajectories may be a result of inadequate

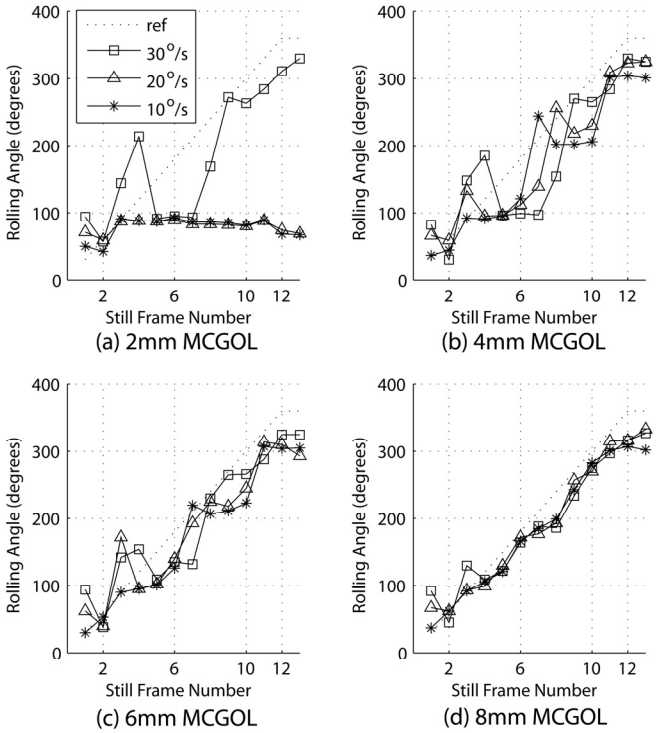

Fig. 6. Still frame analysis results for level surface rolling showing measured Rolling Angle trajectories for Max. CG Offset Lengths of (a) 2 mm, (b) 4 mm, (c) 6 mm, and (d) 8 mm.

TABLE 2
ROLLING ANGLE ERROR RMS (DEGREES) FOR CCGOAR TRAJECTORIES ON A LEVEL SURFACE.

Constant CG Offset Angle Rate (°/s)	Max. CG Offset Lengths (mm) 2	4	6	8
30	65	61	43	36
20	153	47	43	27
10	152	48	41	26

TABLE 3
SUCCESS RATE OUT OF FIVE EXPERIMENTS FOR CCGOAR TRAJECTORIES ON A LEVEL SURFACE.

Constant CG Offset Angle Rate (°/s)	Max. CG Offset Lengths (mm) 2	4	6	8
30	5	5	5	5
20	2	4	3	5
10	0	5	5	5

TABLE 4
ENERGY USAGE PER METER TRAVELED (J/M) FOR CCGOAR TRAJECTORIES ON A LEVEL SURFACE.

Constant CG Offset Angle Rate (°/s)	Max. CG Offset Lengths (mm) 2	4	6	8
30	38	46	53	63
20	56	65	71	78
10	67	102	98	111

dynamic influence due to slower rolling and joint rates combined with smaller MCGOL.

C. Walking Experiments

For comparison with rolling, walking experiments were performed for simple flipping and inchworm type gaits on a level surface as demonstrated in Fig. 7a and Fig. 7b respectively. The flipping gait studied here is an extension to that already developed for the RDB [2], and the inchworm gait is common to climbing robots with similar morphologies [10-12]. For both gaits, the joint trajectories for a single step consist of two trajectory points: the initial and final configurations. This is intended to reduce power consumption by eliminating the need to servo along the trajectory and to increase speed. Electro-magnetic grippers are used to grip the ferrous walking surface.

Ten experiments were performed for each gait type for averaging purposes. Energy consumption on a per meter basis and average translational speed data for both walking trajectories are presented in Table 5 as averages of the ten experiments. It can be seen that the inchworm walking gait performs very poorly compared to the flipping walking gait, again likely due to the large amount of friction in the gear train. Simply put, the inchworm gait requires greater joint articulations per unit distance traveled, and therefore more energy.

D. Comparison of Locomotion Modes

Rolling experiment data are included alongside walking experiment data in Table 5 for purposes of comparison. We have included data from the experiments producing the greatest energy efficiency, greatest translational speed, and best rolling trajectory tracking (2.0 mm MCGOL - 30°/s CCGOAR, 2.0 mm MCGOL - 30°/s CCGOAR, and 8.0 mm MCGOL - 10°/s CCGOAR respectively). It can be seen that quasi-static rolling is not capable of translational speeds as fast as the flipping gait, though it provides significant improvement in energy usage over both types of walking gaits. When magnets are used as grippers, the energy required for rolling is 26% of that of a flipping walking gait (the most efficient of the walking gaits studied here). When gripper energy consumption is neglected, the motors alone use 14% less of the energy of a flipping walking gait for rolling—still a significant improvement.

V. CONCLUSIONS AND FUTURE WORK

We have shown that the hybridization of rolling with walking is capable of increasing the energy efficiency of walking robots. Tests of our quasi-static rolling controller on the RDB robot have proven capability of increasing energy efficiency by as much as a factor of 3.9 over walking using magnetic grippers. When only motor energy consumption is considered, we show a 14% decrease in energy consumption for rolling over walking. These features allow such hybrid robots the ability to better adapt to their operational environment by selecting the mode of locomotion most

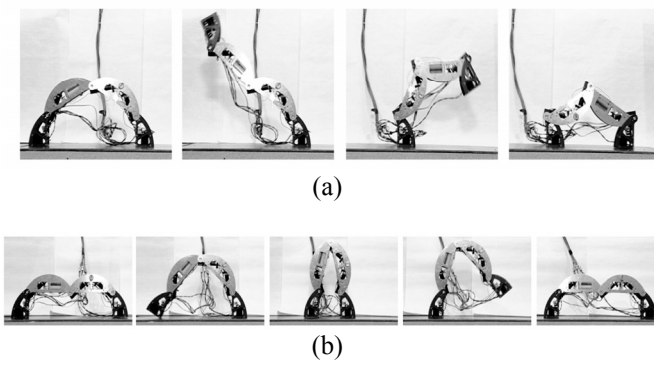

Fig. 7. Demonstration of (a) flipping and (b) inchworm type walking gaits.

appropriate: walking locomotion affords the benefits of being able to walk or climb over obstacles and scaling vertical surfaces, while quasi-static rolling locomotion is capable of greater energy efficiency and locomotion on surfaces which the robot cannot grip.

Because the RDB is primarily intended as a climber, motor and gearing selections were based heavily on the requirements of climbing. Specifically, the motors and gearing were selected to allow for joint motion when in the full cantilever position. This high joint torque requirement for climbing is in conflict with the desire for greater joint speed for rolling which would facilitate faster and more dynamic modes of rolling. The large gear reduction is also a detriment to all forms of locomotion because of inherent inefficiency in the gear train. Future work will include reevaluation/optimization of the motor and gearing selection with the intent to increase joint speeds, decrease gearing inefficiency, and still allow for climbing on vertical surfaces.

Though our quasi-static rolling controller has not demonstrated the ability to provide translational speeds greater than walking, our future work is to include development of control for more dynamic methods of rolling. These methods could include: using the legs to kick off the ground, joint articulations to pump momentum into the system, and using CG offsets to sustain large torques. We intend to implement feedback control which will require the development of a sensor suite for state estimation and perhaps terrain characterization. The tether and off-board controller will be replaced with an embedded controller. We will study transitions between locomotion modes and terrain characterization to enable selection of the mode most appropriate. Finally we intend to utilize our experience with the RDB on the more versatile spherical HAB robot and future design iterations of the RDB.

REFERENCES

[1] B. Shores and M. Minor, "Design, Kinematic Analysis, and Quasi-Steady Control of a Morphic Rolling Disk Biped Climbing Robot," presented at IEEE Int'l Conf. on Rob. and Autom (ICRA 05), Barcelona, Spain, 2005.

[2] B. E. Shores, "Hybrid locomotion for enhanced mobility in robotic systems," in Mechanical Engineering. Salt Lake City: University of Utah, 2005, pp. 194.

[3] C. C. Phipps and M. A. Minor, "Introducing the Hex-A-Ball, a Hybrid Locomotion Terrain Adaptive Walking and Rolling Robot," presented at CLAWAR 2005, London, U.K., 2005.

[4] A. Halme, T. Schonberg, and Y. Wang, "Motion control of a spherical mobile robot," presented at Proceedings of the 1996 4th International Workshop on Advanced Motion Control, AMC'96. Part 1 (of 2), Mar 18-21 1996, Tsu, Jpn, 1996.

[5] R. Mukherjee and T. Das, "Feedback stabilization of a spherical mobile robot," presented at IROS 2002: IEEE/RSJ International Conference on Intelligent Robots and Systems, Lausanne, Switzerland, 2002.

[6] M. Yim, "New locomotion gaits," presented at Proceedings of the 1994 IEEE International Conference on Robotics and Automation, 8-13 May 1994, San Diego, CA, USA, 1994.

[7] T. Yamawaki, O. Mori, and T. Omata, "Nonholonomic dynamic rolling control of reconfigurable 5R closed kinematic chain robot with passive joints," presented at IEEE International Conference on Robotics and Automation. IEEE ICRA 2003 Conference Proceedings, 14-19 Sept. 2003, Taipei, Taiwan, 2003.

[8] W. H. Lee and A. C. Sanderson, "Dynamic rolling locomotion and control of modular robots," IEEE Transactions on Robotics and Automation, vol. 18, pp. 32-41, 2002.

[9] J. Denavit, and Hartenberg, R.S., "A kinematic notation for lower pair mechanisms based on matrices," J. Applied Mechanics, vol. 22, pp. 215-221, 1955.

[10] M. Minor, H. Dulimarta, G. Danghi, R. Mukherjee, R. L. Tummala, and D. Aslam, "Design, implementation, and evaluation of an under-actuated miniature biped climbing robot," presented at 2000 IEEE/RSJ International Conference on Intelligent Robots and Systems, Oct 31-Nov 5 2000, Takamatsu, 2000.

[11] M. A. Minor and R. Mukherjee, "Under-actuated kinematic structures for miniature climbing robots," Journal of Mechanical Design, Transactions of the ASME, vol. 125, pp. 281-291, 2003.

[12] S. P. Krosuri and M. A. Minor, "Design, modeling, control, and evaluation of a hybrid hip joint miniature climbing robot," International Journal of Robotics Research, vol. 24, pp. 1033-1053, 2005.

TABLE 5
COMPARISON OF LOCOMOTION MODES, MOST FAVORABLE VALUES ARE HIGHLIGHTED IN BOLD.

		Flipping	Inchworm	Efficient Rolling	Fast rolling	Best Tracking Rolling
Energy Consumption (J/m)	Motors	44	82	38	38	111
	Magnets	105	253	NA	NA	NA
	TOTAL	149	335	**38**	**38**	111
Average Translational Speed (m/s)		**0.136**	0.032	0.057	0.057	0.019